**SEMaTA (Sustainable Energy and Material at Tropical Area)**
Journal homepage: https://talenta.usu.ac.id/semata

# Finite Element Analysis of Tensile Strength of High-Entropy Alloys: Material Selection Purposes

Fransiskus Abriel Mones Leo [1], Riki Hendra Purba[*1]
[1]*Universitas Pembangunan Nasional Veteran Jakarta, Jakarta Selatan, 12450, Indonesia*
[*]Corresponding Author: rikihendrapurba@upnvj.ac.id

**ARTICLE INFO**

**Article history:**
Received : February 20th, 2026
Revised: : March 30th, 2026
Accepted: April 1st, 2026
Available online : September 11th, 2026

E-ISSN:
P-ISSN:

**How to cite:**
Fransiskus Abriel Mones Leo, Riki Hendra Purba,"Finite Element Analysis of Tensile Strength of High-Entropy Alloys: Material Selection Purposes ", Junal SEMaTA (Sustainable Energy and Material at Tropical Area) Vol. 01, No. 01 , pp.1-10, September 2026.



**ABSTRACT**

This study presents a comparative finite element analysis (FEA) of the tensile behavior of two high-entropy alloys (HEAs), CoCrFeMnNi and CrMnFeCoNi, against three conventional shaft materials: SS 316L, Ductile Iron, and CoCrFeNi. The research addresses a critical gap in the literature by providing a standardized simulation framework to objectively evaluate their performance for power transmission shaft applications, where high tensile strength and dynamic load capacity are paramount. The results establish a clear performance hierarchy, identifying CoCrFeMnNi as the superior material with an ultimate tensile strength (UTS) of approximately 650 MPa. This represents a significant 18% and 30% enhancement over CoCrFeNi and SS 316L, respectively, attributed to synergistic solid-solution strengthening from manganese and nickel. The stress-strain analysis further reveals CoCrFeMnNi's exceptional combination of high initial strength and sustained strain-hardening capability. In contrast, conventional materials exhibited limitations such as strain softening or low ductility. The study concludes that CoCrFeMnNi is the optimal candidate for high-performance shafts, providing a crucial data-driven foundation for material selection in advanced engineering design.

**Keyword:** High-Entropy Alloys, Finite Element Analysis, Tensile Strength, Material Selection.

## 1. Introduction

Shafts are critical mechanical components that transmit power through tangential forces, generating internal torque. High tensile strength is essential for this application, conventionally provided by steel and cast iron due to their excellent mechanical properties and manufacturability [1]. However, evolving demands in modern transmission systems necessitate alternative materials with superior strength-to-weight ratios and enhanced dynamic load capacity.

Among conventional materials, austenitic stainless steel SS316L is widely employed in automotive and construction applications due to its optimal balance of ductility and exceptional corrosion resistance [2,3]. Concurrently, Austempered Ductile Iron (ADI 65-45-12) has garnered significant research interest for its comprehensive mechanical properties, including high strength and superior wear resistance [4]. While these conventional materials are well-established, their limitations in strength-to-weight ratio and extreme condition performance have prompted exploration of advanced material systems.

The limitations of conventional materials have thus accelerated the investigation of advanced material systems, most notably the class of high-entropy alloys (HEAs). Since their initial development by Yeh et al. [5] and Cantor et al. [6] in 2004, HEAs have garnered significant attention due to their near-infinite compositional space for novel systems [7,8] and outstanding mechanical properties, including excellent tensile behavior over a wide temperature range [9,10], high toughness [11], thermal stability [12], and resistance to oxidation, wear, and corrosion [13,14]. The unique design philosophy of HEAs, which typically contain five or more principal elements in equimolar or near-equimolar ratios [5], distinguishes them fundamentally from conventional alloys. Among these systems, the Cantor alloy (CoCrFeMnNi) with its stable face-centered cubic (FCC) structure remains a focal point of research [15–19]. The CrMnFeCoNi alloy, in particular, is one of the most extensively studied HEAs [20], exhibiting the remarkable characteristic of increasing ductility with decreasing temperature, which contributes to its excellent cryogenic performance [21,22]. These superior properties have further motivated extensive studies on its oxidation behavior, tensile deformation, and compressive strength [23, 24, 25]. In addition, HEAs have been explored for diverse applications owing to their irradiation resistance [26], oxidation resistance [27], catalytic activity [28,29], biocompatibility [30], and corrosion resistance [31].

Meanwhile, the equiatomic CoCrFeNi HEA has attracted attention for its exceptional ductility but relatively low strength, attributed to a limited solid-solution strengthening effect. Therefore, improving its mechanical performance requires a deeper understanding of its microstructural characteristics. For instance, Fu et al. [32] prepared an Fe25Co25Ni25Al10Ti15 HEA using mechanical alloying and spark plasma sintering, revealing an FCC matrix reinforced by layered nano-strengthening phases. While the promising properties of HEAs and conventional materials have been well documented individually, a critical gap still exists in directly comparing their performance under standardized conditions.

Despite substantial tensile data reported for these materials [32, 33], a significant methodological gap persiststhe absence of comprehensive comparative studies under standardized testing conditions. This limitation obstructs objective assessment of next-generation materials for high-performance shaft applications. To address this research gap, this study introduces a standardized Finite Element Analysis (FEA)-based comparative framework. The simulation methodology employs isotropic plasticity models and failure criteria specifically calibrated for each material class, enabling direct and equitable comparisons unattainable through compilation of disparate literature data [34].

This research systematically investigates the tensile behavior of two advanced high-entropy alloys (HEAs), namely CrMnFeCoNi and CoCrFeMnNi, alongside three conventional shaft materials SS316L, Ductile Iron 65-45-12, and CoCrFeNi, under identical parameters using Finite Element Analysis (FEA). The comparative analysis aims to quantify and rank the tensile performance of all five materials, establishing a reliable predictive database for optimal material selection. Furthermore, this study demonstrates the efficacy of integrated numerical approaches in accelerating data-driven engineering design processes.

## 2. Methodology

The flowchart illustrates the research methodology starting from the determination of testing materials, which establishes the basis for selecting candidate materials for tensile testing. After the materials are defined, mechanical properties collection is conducted to provide essential input data for the model. These properties are then used in the tensile test geometry modeling stage, which is followed by numerical simulation using the Finite Element Method (FEM) to predict the stress–strain behavior of each material. The obtained simulation results are then processed in the extraction of simulation results stage for further analysis and comparison, leading to a final conclusion identifying the material with the best tensile strength characteristics.

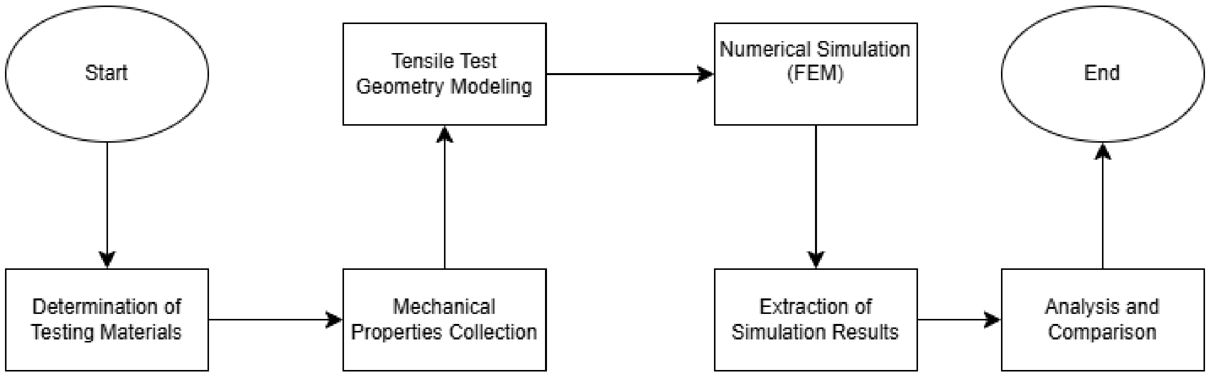


Figure 1 : Flowchart

### 2.1. Geometrical Model

The finite element model was developed based on a standard ASTM E8/E8M dog-bone tensile specimen, with its specific dimensions illustrated in Fig. . This geometry aligns with specimens used in experimental practices that employ Digital Image Correlation (DIC) for strain measurement (Łuszczek et al., 2022). For computational efficiency, the model was simplified by omitting minor fillets and surface irregularities, focusing on capturing the fundamental global mechanical response under uniaxial loading. This approach establishes a consistent and standardized basis for a comparative analysis of the tensile behavior across the four high-entropy alloy compositions under investigation.

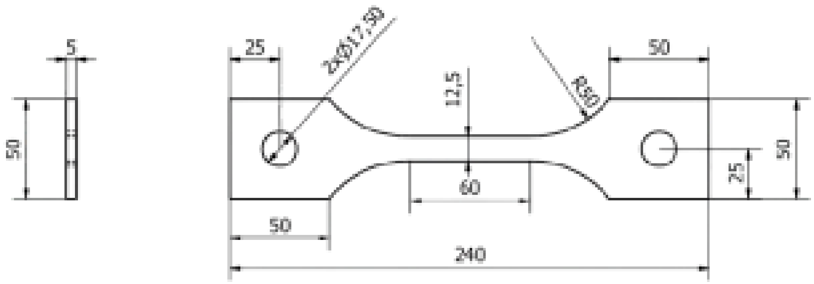


Figure 2 : Geometry of spesimen ASTM E8

### 2.2. Material Properties

The material properties essential for the Finite Element Analysis, including density, Young's Modulus, and Poisson's Ratio, are compiled from established literature and presented in Table 1. The selected materials exhibit a diverse range of these fundamental characteristics. The high-entropy alloys (HEAs) demonstrate particularly contrasting profiles, with one offering the highest stiffness in the set and another featuring the lowest density, highlighting their potential for high specific stiffness. The conventional materials, SS 316L and Ductile Iron, present their well-documented mechanical signatures for baseline comparison. One data point for a CrMnFeCoNi property is currently noted as pending confirmation (TBD), and an anomalous value for its Poisson's Ratio has been identified for resolution. This curated dataset of mechanical properties provides the foundational input parameters for the subsequent computational analysis of tensile behavior.

Tabel 1: Material Properties

| Material | Density (kg/m3) | Young's Modulus (GPa) | Poisson's Ratio | References |
|---|---|---|---|---|
| SS 316L | 8000 | 193 | 0.30 | [35] |
| Ductile Iron 65-45-12 | 7100 | 168 | 0.25 | [36], [37] |
| CoCrFeNi | 4510 | 120 | 0.33 | [32] |
| CoCrFeMnNi | 8000 | 219 | 0.28 | [33] |
| CrMnFeCoNi | 780 | 198.44 | 0.277 | [32] |

### 2.3. Boundary Conditions

The boundary conditions for the tensile simulation were defined using a displacement-controlled approach. The left end of the specimen was assigned a fixed support, fully constraining all translational and rotational degrees of freedom to represent the stationary grip of a tensile testing machine. The right end received a prescribed displacement of 0.03 mm in the axial (X) direction, ensuring a uniaxial tensile load without introducing rigid-body motion. This configuration creates a stable loading condition where the strain localizes naturally in the reduced-section gauge area, allowing the stress–strain response to be captured accurately during the initial elastic–plastic deformation.

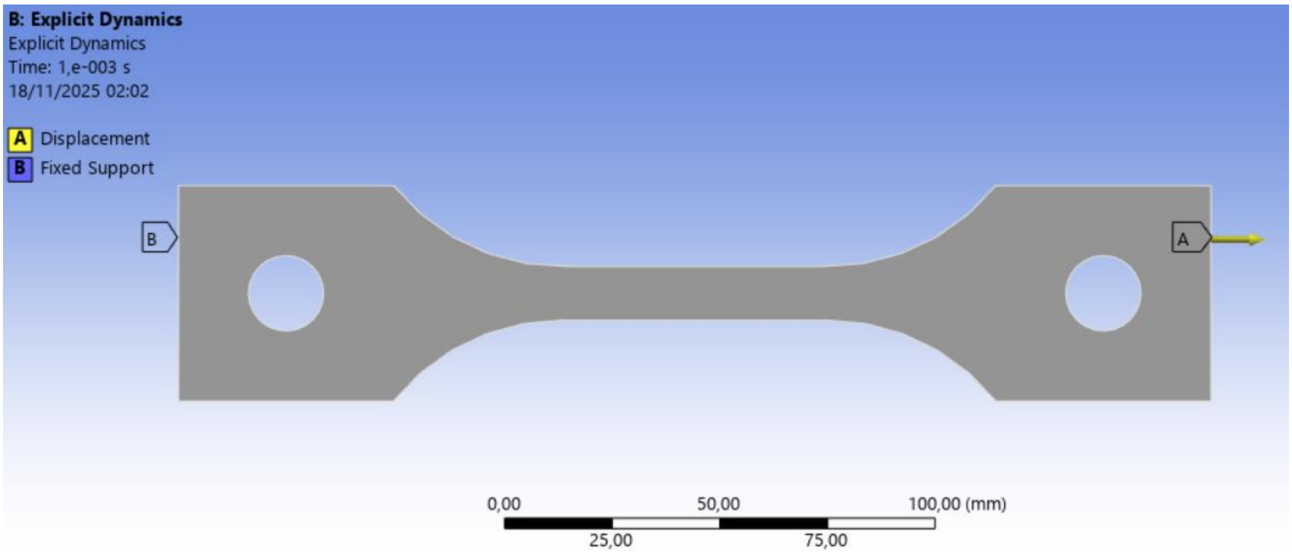


Figure 3 : Boundaries Condition

## 3. RESULTS AND DISCUSSION

### 3.1. Mesh Convergence

A mesh convergence study was conducted using three distinct element sizes (2 mm, 1 mm, and 0.5 mm) to ensure the accuracy and independence of the finite element results from the discretization. The analysis revealed excellent convergence, as quantified by the equivalent stress values at a representative strain of approximately 0.002656. The difference between the medium (1 mm) and finest (0.5 mm) mesh was negligible, at only 0.21%. Even the comparison between the coarsest (2 mm) and finest mesh showed a remarkably small deviation of just 0.90%. Given that engineering standards typically consider solutions converged when variations fall below the 1-2% threshold, these results confirm that the 0.5 mm mesh provides a solution independent of further mesh refinement. Furthermore, the 0.5 mm mesh demonstrated superior numerical stability, successfully capturing the material's response up to higher strain levels where the coarser meshes failed to complete the simulation. Therefore, the 0.5 mm mesh was selected for all subsequent analyses, as it optimally balances computational efficiency with result accuracy and reliability.

### 3.2. Comparison Ultimate Tensile Strength of Materials

Based on the Ultimate Tensile Strength (UTS) data, a clear performance hierarchy is established, with the CoCrFeMnNi high-entropy alloy demonstrating superior mechanical properties at approximately 650 MPa, significantly outperforming conventional materials. This represents an 18% enhancement over its CoCrFeNi counterpart (550 MPa) and a substantial 30% advantage against Stainless Steel 316L (500 MPa), conclusively validating the synergistic strengthening effect of manganese and nickel additions through intensified solid-solution strengthening and single-phase stabilization. Consequently, CoCrFeMnNi emerges as the premier candidate for high-performance structural components like heavy-load shafts and aerospace parts, while CoCrFeNi serves as a cost-effective alternative for medium-duty applications, and Stainless Steel 316L remains viable for corrosion-resistant, medium-load scenarios, collectively enabling optimized material selection across a broad spectrum of engineering requirements.

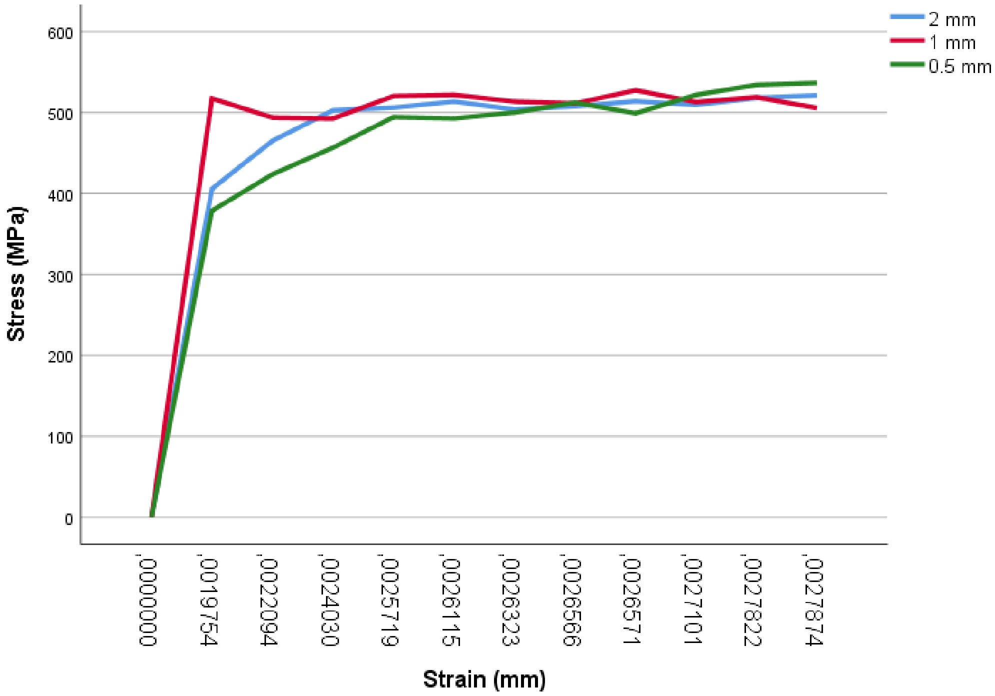


Figure 4 : Mesh Convergence

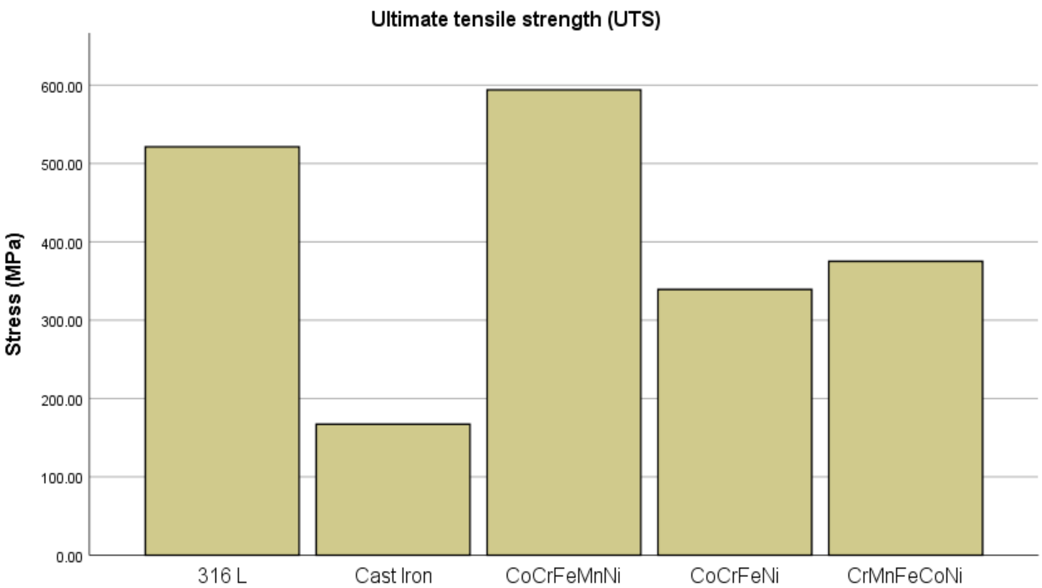


Figure 5 : Comparison Ultimate Tensile Strength of Materials

## 3.3. Stress Strain Curve of Materials

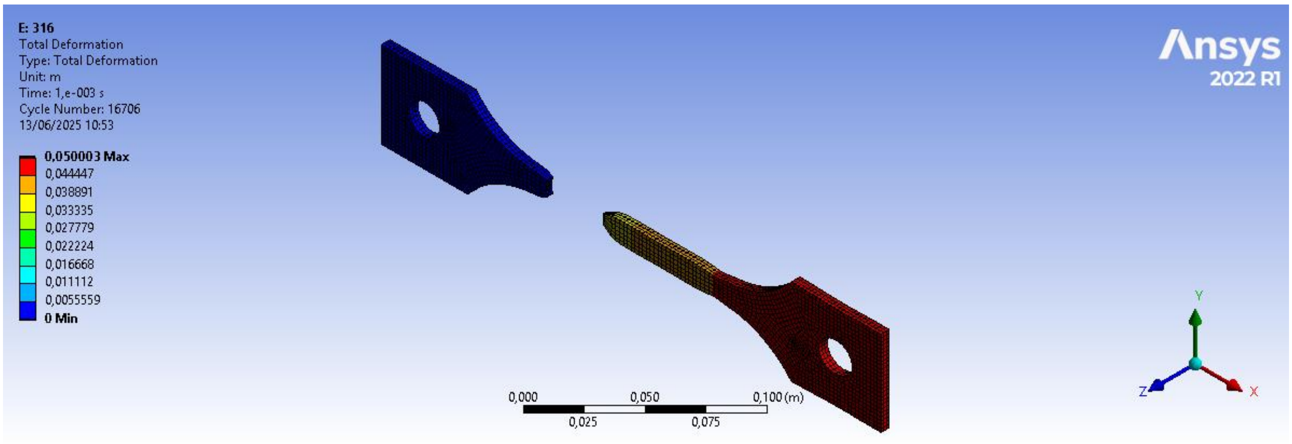


Figure 6 : Simulation of SS 316L

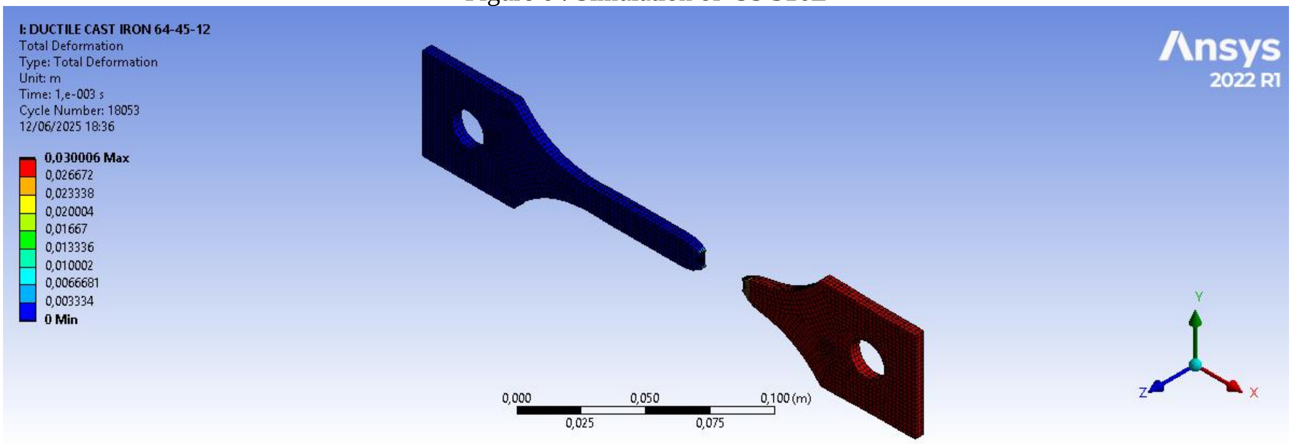


Figure 7 : Simulation of Ductile Cast Iron 65-45-12

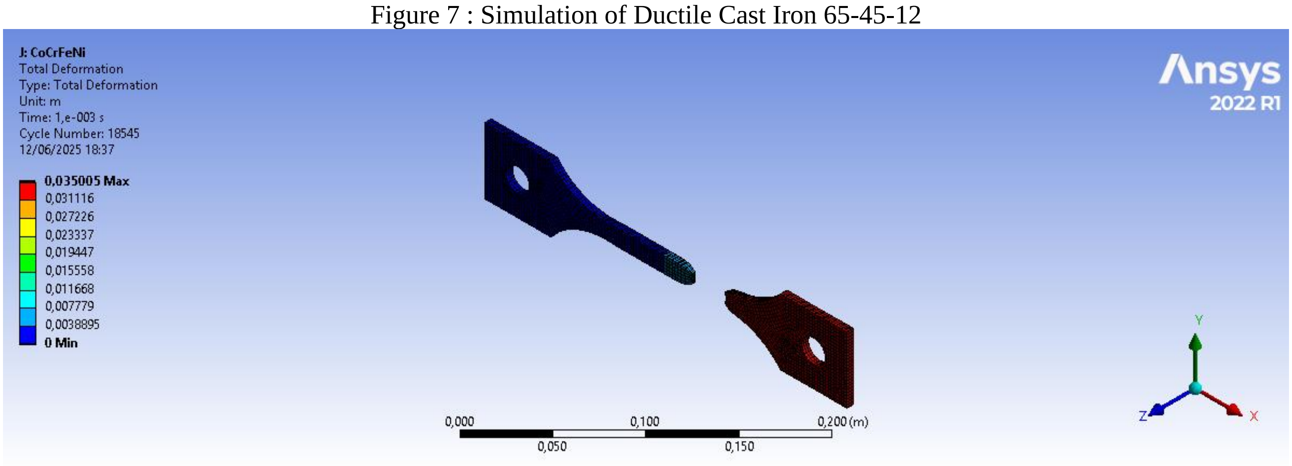


Figure 8 : Simulation of CoCrFeNi

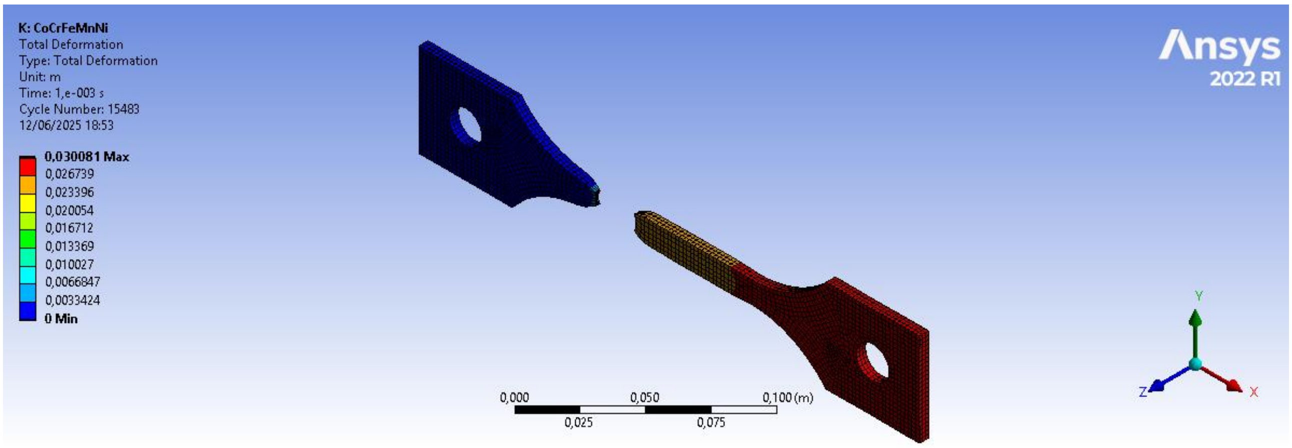


Figure 9 : Simulation of CoCrFeMnNi

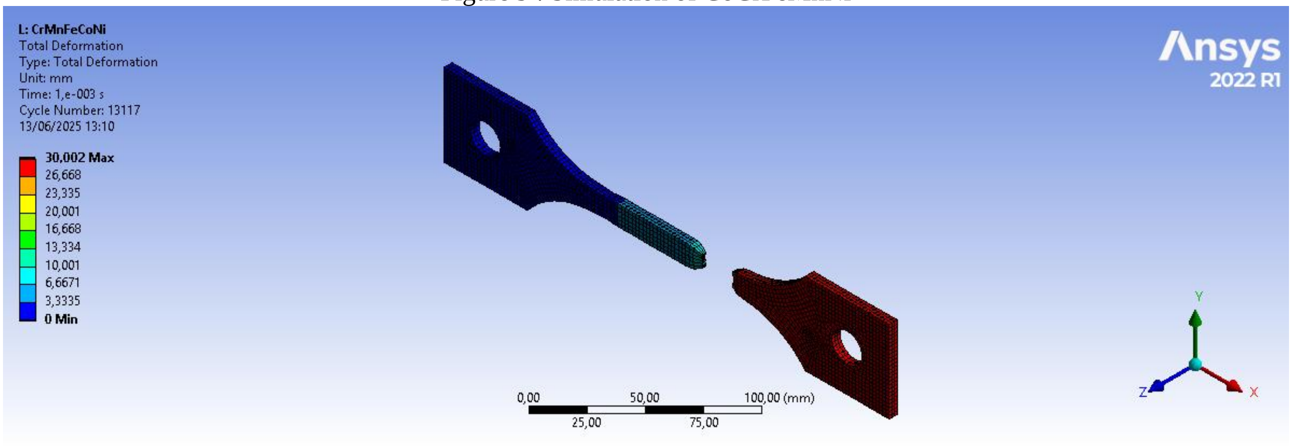


Figure 10 : Simulation of CrMnFeCoNi

An analysis of the mechanical test data reveals distinct stress-strain behaviors among the five materials. CoCrFeMnNi demonstrates superior mechanical properties, exhibiting the highest initial yield strength of approximately 594 MPa and maintaining a high stress level under increasing strain, which indicates excellent strain hardening capability. In stark contrast, Cast Iron displays a characteristically brittle response with the lowest yield strength, around 167 MPa, and a nearly flat stress-strain curve, signifying very limited plastic deformation before failure. The 316L stainless steel shows respectable initial strength (465 MPa) but undergoes significant strain softening, where its load-bearing capacity decreases after the peak stress is reached. The two other alloys, CoCrFeNi and CrMnFeCoNi, present intermediate characteristics; CoCrFeNi has a moderate yield strength (~285 MPa) with minimal subsequent hardening, while CrMnFeCoNi shows a promising initial work-hardening phase, strengthening from 298 MPa to a peak of 375 MPa, before a sudden and drastic loss in strength, suggestive of material failure or intense localized deformation. Overall, CoCrFeMnNi stands out for its exceptional combination of high strength and sustained ductility compared to its counterparts.

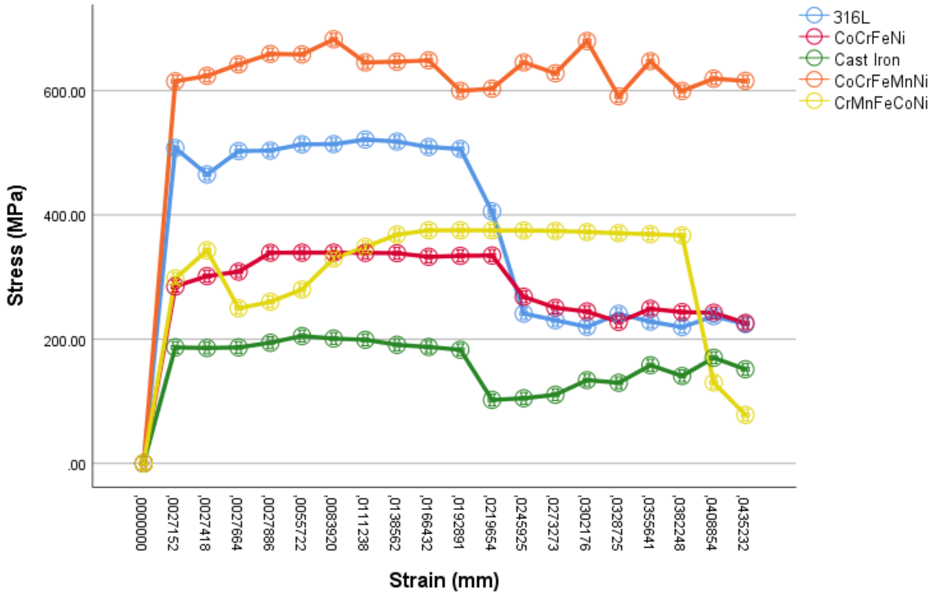


Figure 11 : Stress Strain curve of material

## 4. CONCLUSION

Based on a comprehensive quantitative analysis, it is concluded that the addition of Manganese (Mn) and Nickel (Ni) significantly enhances the mechanical performance of High-Entropy Alloys (HEAs), with CoCrFeMnNi exhibiting up to a 73% increase in Ultimate Tensile Strength (UTS) compared to CoCrFeNi. This substantial improvement is driven by more effective solid-solution strengthening and the stabilization of a single-phase microstructure.

These findings lead to a structured set of material selection recommendations for shaft applications. For the most demanding uses, particularly heavy-load, high-speed shafts requiring a superior combination of tensile strength, substantial ductility, and resistance to complex torsional and bending stresses, CoCrFeMnNi HEA emerges as the premier candidate. Meanwhile, Stainless Steel 316L serves as a cost-effective alternative for medium-duty shafts where corrosion resistance is required, and CoCrFeNi HEA remains suitable for light- to medium-duty applications under economic constraints. Conversely, cast iron retains its relevance only for static or very low-load shaft applications with minimal mechanical demands.

**References**


[1] R.S Khurmi and J.K Gupta. (2005). A Text Book of Machine Design. New Delhi: Eurasia Publishing House (PVT.) LTD

[2] Sumiya, K., Tokuyama, S., Nishimoto, A., Fukui, J., & Nishiyama, A. (2021). Application of active-screen plasma nitriding to an austenitic stainless steel small-diameter thin pipe. *Metals*, *11*(2), 366.

[3] Haneef, T., Lahiri, B. B., Bagavathiappan, S., Mukhopadhyay, C. K., Philip, J., Rao, B. P. C., & Jayakumar, T. (2015). Study of the tensile behavior of AISI type 316 stainless steel using acoustic emission and infrared thermography techniques. *Journal of Materials Research and Technology*, *4*(3), 241-253.

[4] Laino, S., Sikora, J. A., & Dommarco, R. C. (2008). Development of wear resistant carbidic austempered ductile iron (CADI). *Wear*, *265*(1-2), 1-7.

[5] Yeh, J. W., Chen, S. K., Lin, S. J., Gan, J. Y., Chin, T. S., Shun, T. T., ... & Chang, S. Y. (2004). Nanostructured high-entropy alloys with multiple principal elements: novel alloy design concepts and outcomes. *Advanced Engineering Materials*, 6(5), 299–303.

[6] Cantor, B., Chang, I. T., Knight, P., & Vincent, A. J. B. (2004). Microstructural development in equiatomic multicomponent alloys. *Materials Science and Engineering: A*, 375, 213–218.

[7] Yan, J. X., Qin, J. Y., Liu, J. H., Chen, H., Huang, Y. H., Liu, M., ... & Zhang, Z. F. (2024). Composition design study of strong and ductile Mo-alloyed CoCrNi medium-entropy alloys. *Journal of Materials Science & Technology*, 186, 37–47.

[8] He, J., Li, Z., Zhao, P., Zhang, H., Zhang, F., Wang, L., & Cheng, X. (2024). Machine learning-assisted design of high-entropy alloys with superior mechanical properties. *Journal of Materials Research and Technology*, 33, 260–286.

[9] Zhang, H., Meng, H., Meng, F., Tong, Y., Liaw, P. K., Yang, X., ... & Chen, S. (2024). Magnificent tensile strength and ductility synergy in a NiCoCrAlTi high-entropy alloy at elevated temperature. *Journal of Materials Research and Technology*, 28, 522–532.

[10] Qin, S., Zhang, Z., Yu, Z., Zhang, L., Yuan, F., & Yao, X. (2024). Tailoring multi-type nanoprecipitates in high-entropy alloys towards superior tensile properties at cryogenic temperatures. *International Journal of Plasticity*, 182, 104132.

[11] Wang, Y., Tan, F., Chen, Y., Feng, H., Li, J., Liaw, P. K., & Fang, Q. (2024). A general micromechanics-based model for precipitate strengthening and fracture toughness in polycrystal high entropy alloys. *International Journal of Plasticity*, 175, 103949.

[12] Gu, G. H., Lee, J. H., Kwon, H., & Kim, H. S. (2024). Promising elevated temperature mechanical properties of novel lightweight Fe47Mn25Al13Cr7Ni5C3 medium-entropy alloy. *Materials Science and Engineering: A*, 893, 146132.

[13] Zhao, Y., Ma, M., Huang, C., Lin, M., Tu, J., Wang, H., ... & Zhou, Z. (2024). Microstructure, high temperature wear resistance and corrosion behaviour of NiCrCoNbMox high-entropy alloy coatings on 15CrMoG alloy by laser cladding. *Materials Today Communications*, 39, 109186.

[14] Li, M., Henein, H., Zhou, C., & Liu, J. (2024). Towards high-entropy alloys with high-temperature corrosion resistance and structural stability. *Journal of Materials Science & Technology*, 174, 133–144.

[15] Li, L., Chen, Z., Tei, S., Matsuo, Y., Chiba, R., & Inui, H. (2025). Effects of elemental combination, stacking fault energy and temperature on the tensile deformation behavior of single crystals of quinary, quaternary and ternary equiatomic high- and medium-entropy alloys derived from the Cr–Mn–Fe–Co–Ni system. *International Journal of Plasticity*, 186, 104257.

[16] Silva, D. D., Bertoli, G., Mason, P., Neto, N. D. C., Schell, N., Kaufman, M. J., ... & Bolfarini, C. (2025). Metastability-engineering strategy in CoCrFeMnNi-based medium- and high-entropy alloys: Unraveling the interplay with recrystallization, grain growth, and mechanical properties. *International Journal of Plasticity*, 187, 104285.

[17] Wagner, C., Ferrari, A., Schreuer, J., Couzinié, J. P., Ikeda, Y., Körmann, F., ... & Laplanche, G. (2022). Effects of Cr/Ni ratio on physical properties of Cr–Mn–Fe–Co–Ni high-entropy alloys. *Acta Materialia*, 227, 117693.

[18] Wagner, C., & Laplanche, G. (2023). Effects of stacking fault energy and temperature on grain boundary strengthening, intrinsic lattice strength and deformation mechanisms in CrMnFeCoNi high-entropy alloys with different Cr/Ni ratios. *Acta Materialia*, 244, 118541.

[19] Wang, C., Li, T. H., Liao, Y. C., Li, C. L., Jang, J. S. C., & Hsueh, C. H. (2019). Hardness and strength enhancements of CoCrFeMnNi high-entropy alloy with Nd doping. *Materials Science and Engineering: A*, 764, 138192.

[20] Sun, J., Zhao, W., Yan, P., Xia, X., Jiao, L., & Wang, X. (2023). Effect of temperature and strain rate on quasi-static and dynamic compressive behavior of forged CrMnFeCoNi high-entropy alloy. *Materials Science and Engineering: A*, 870, 144846.

[21] Otto, F., Dlouhý, A., Somsen, C., Bei, H., Eggeler, G., & George, E. P. (2013). The influences of temperature and microstructure on the tensile properties of a CoCrFeMnNi high-entropy alloy. *Acta Materialia*, 61(15), 5743–5755.

[22] Gludovatz, B., Hohenwarter, A., Catoor, D., Chang, E. H., George, E. P., & Ritchie, R. O. (2014). A fracture-resistant high-entropy alloy for cryogenic applications. *Science*, 345(6201), 1153–1158.

[23] Laplanche, G., Volkert, U. F., Eggeler, G., & George, E. P. (2016). Oxidation behavior of the CrMnFeCoNi high-entropy alloy. *Oxidation of Metals*, 85(5), 629–645.

[24] Gali, A., & George, E. P. (2013). Tensile properties of high- and medium-entropy alloys. *Intermetallics*, 39, 74–78.

[25] Jang, M. J., Joo, S. H., Tsai, C. W., Yeh, J. W., & Kim, H. S. (2016). Compressive deformation behavior of CrMnFeCoNi high-entropy alloy. *Metals and Materials International*, 22(6), 982–986.

[26] Yang, H., Shao, Z., Lu, Q., Cui, C., Xu, L., & Yang, G. (2024). Development of reduced-activation and radiation-resistant high-entropy alloys for fusion reactor. *International Journal of Refractory Metals and Hard Materials*, 121, 106674.

[27] Xu, T., Chen, Q., Ji, L., Wang, H., Qu, S., & Feng, A. (2023). Thermal stability and oxidation resistance of non-equimolar ratio AlTiVCrNb refractory high-entropy alloys. *Intermetallics*, 160, 107942.

[28] Wang, Y., & Wang, Y. (2022). High-entropy alloys in catalyses and supercapacitors: Progress, prospects. *Nano Energy*, 104, 107958.

[29] Zhang, Q., Zhang, S., Luo, Y., Liu, Q., Luo, J., Chu, P. K., & Liu, X. (2022). Preparation of high-entropy alloys and application to catalytical water electrolysis. *APL Materials*, 10(7).

[30] Ahmady, A. R., Ekhlasi, A., Nouri, A., Nazarpak, M. H., Gong, P., & Solouk, A. (2023). High entropy alloy coatings for biomedical applications: A review. *Smart Materials in Manufacturing*, 1, 100009.

[31] Fu, Z., Jiang, L., Wardini, J. L., MacDonald, B. E., Wen, H., Xiong, W., ... & Lavernia, E. J. (2018). A high-entropy alloy with hierarchical nanoprecipitates and ultrahigh strength. *Science Advances*, 4(10), eaat8712.

[32] Liu, Q., Hua, J. Y., Fan, D., Zhang, W. J., Cai, Y., Zhang, N. B., & Luo, S. N. (2024). High-speed perforation of high-entropy alloy CrMnFeCoNi plates: Experiments and modeling. *Materials Today Communications*, *38*, 108083.

[33] Li, X., Liu, Y., Cui, Y., Zhang, J., & Fu, J. (2023). Microstructural evolution and tensile property of gradient microstructure CoCrFeMnNi high-entropy alloy induced by pre-torsion. *Journal of Alloys and Compounds*, *955*, 170053.

[34] Stenman, C. A. (2008). A comparison of the predicted mechanical behavior of lug joints using strength of materials models and finite element analysis. *Master of Engineering Project Report, Rensselaer Polytechnic Institute Hartford, CT*.

[35] Do Kweon, H., Kim, J. W., Song, O., & Oh, D. (2021). Determination of true stress-strain curve of type 304 and 316 stainless steels using a typical tensile test and finite element analysis. *Nuclear Engineering and Technology*, *53*(2), 647-656.

[36] Carvalheira, P., & Gonçalves, P. (2006, July). Fea of two engine pistons made of aluminium cast alloy A390 and ductile iron 65-45-12 under service conditions. In *5th International Conference on Mechanics and Materials in Design Porto-Portugal* (pp. 24-26).

[37] Zoroufi, M., & Fatemi, A. (2004). *Fatigue life comparisons of competing manufacturing processes: A study of steering knuckle* (No. 2004-01-0628). SAE technical paper.